Water Air Soil Pollut (2023) 234:664
https://doi.org/10.1007/s11270-023-06683-0

Evaluation of Methylene Blue Adsorption onto Lignocellulosic Biomass (Raw *Rumex Crispus* L. Stem): Characterization, Kinetics, and Isotherms

Erbil Kavcı

Received: 29 May 2023 / Accepted: 29 September 2023 / Published online: 16 October 2023

Abstract Worldwide water sources continue to be polluted daily by various additives, of which dyestuffs are a significant contributing factor. In the present study, *Rumex Crispus* L. (RCL) was used as a biomass bio-adsorbent, and the adsorption of methylene blue on RCL was investigated. RCL was characterized using Brauner–Emmett–Teller, Fourier transform infrared, X-ray diffraction, and scanning electron microscopy (SEM) analyses. The effects of the RCL amount (0.5–6 g/L), initial pH (3–10), concentration (40–200 mg/L), contact time (0–60 min), and temperature (293–313 K) on adsorption activities were investigated, and the point of zero charge value of the adsorbent was determined. Thermodynamic studies have shown that adsorption occurs spontaneously and exothermically ($\Delta G^0 = -2.19$ to -0.72 kJ/mol, $\Delta H^0 = -23.8$ kJ/mol, $\Delta S^0 = -0.074$ kJ/mol). Pseudo-first-order, pseudo-second-order, intraparticle diffusion, and Elovich kinetic models were tested, and the kinetic data were examined. The kinetic data showed that the pseudo-second-order kinetic model was the best fit ($R^2 = 0.999$). Tests were conducted using Langmuir and Freundlich models from the isotherm studies. Our data showed good agreement with the Langmuir isotherm model ($R^2 = 0.998$). The maximum adsorption capacity of the RCL monolayer was determined as 50 mg/g according to the Langmuir isotherm model.

Keywords Biomass · Biosorption · Isotherm · Kinetics · Methylene blue · *Rumex Crispus* L

1 Introduction

Individual consumption of manufactured goods has been rapidly increasing in recent years; therefore, many industries from textiles, paper, and cosmetics to leather, food, and plastics are producing more to meet this higher demand. Dyestuffs are the organic compounds used as coloring agents in those manufacturing processes, but it is discharged into the environment with the wastewater after processing, contaminating the potable water (Sarkar et al. 2021). Water pollution leads to a disruption of the ecological balance because these dyestuffs transported to the environment with the wastewater contaminate the soil, harm the aquatic environment and living beings, and reduce the quality and potential use of the water (Bingöl 2022). In addition, many dyestuffs are carcinogenic, mutagenic, and toxic. Human skin diseases lead to disorders in the functioning of organs and nervous and reproductive systems. These substances are also responsible for the development of cancer cells by causing mutations (Isik et al. 2022). Because of their stable structure, dyestuffs do not decompose in water and are visible even at very low

E. Kavcı (✉)
Department of Chemical Engineering, Collage of Engineering and Architecture, Kafkas University, 36100 Kars, Turkey
e-mail: erbilkavci@gmail.com

concentrations; therefore, these organic compounds pose a great threat to the environment and health.

According to the United Nations, more than 2 billion people will not have access to clean water, and 1.8 billion people will experience water scarcity by 2025 (Khan and Khan 2021). Today, water is becoming more and more important for our world, and the polluting dyestuffs in the wastewater must be removed before the wastewater is discharged into the environment (Eldeeb et al. 2022). The methylene blue (MB) used in this study is a cationic dye currently used in dyeing paper, hair, fabric, and cotton. The chemical structure of MB is complex and is resistant to biodegradation (Tang et al. 2021), and MB is chemically stable and has a high solubility in water (Xue et al. 2022). Wastewater, including MB, can pose a threat to living things when exposed to nature, and it can cause various human health problems such as tissue necrosis, precordial pain, vomiting, dizziness, and jaundice (Motejadded Emrooz et al. 2021; Mussa et al. 2023; Thakur et al. 2016).

There are various techniques to remove dyestuffs from solution, such as electrocoagulation (Abdulrazzaq et al. 2021), photocatalytic degradation (Badvi and Javanbakht 2021), oxidation (Muniyasamy et al. 2020), membrane separation (J. Li et al. 2019), chemical precipitation (Beluci et al. 2019), flocculation (Sultana et al. 2021), and adsorption. Of these, adsorption is a low-cost, simple, and efficient removal method. The effectiveness of the adsorption process depends on the dyestuff, operational conditions, as well as the adsorbent used (Fabryanty et al. 2017; Sah et al. 2022); therefore, many studies are being conducted on dyestuff removal using numerous plant-based adsorbents (Akkari et al. 2021; Cheruiyot et al. 2019; Jawad et al. 2019; Nayak and Pal 2020; Sarkar et al. 2021). The adsorbent used in the present study, *Rumex Crispus* L. (RCL), also known as Curly dock, is an invasive weed belonging to the Polygonaceae family that grows up to 40–120-cm long in Europe, North Africa, Iran, Turkey, and Central and Eastern Asia. I used the roots of this plant in folk medicine to treat internal bleeding, rheumatism, and some skin diseases (Idris et al. 2017). They collected its leaves in spring and consumed as a vegetable (Feduraev et al. 2019; Idris et al. 2017). RCL is a very widely grown plant (Bhandari and Park 2022). RCL is a non-cultivated plant (Zahirnejad et al. 2017), but it grows abundantly every year spontaneously in Turkey (Uzun and Demirezer 2019). The leaves of this plant, which grows by itself and easily, are gathered and consumed by some in spring, leaving most of the remaining parts of the plant to decompose in the soil. Thus, it is proposed that this free and easily available biomass could be used as an environmentally friendly adsorbent for dyestuff removal.

In this study, the use of RCL stems as an adsorbent to remove MB from water was investigated. RCL has been characterized using Fourier transform infrared (FTIR) technology, scanning electron microscopy (SEM), the Brauner–Emmett–Teller (BET) method, and X-ray diffraction (XRD). The pH, adsorbent amount, initial concentration, contact time, effect of temperature parameters, and isotherm, kinetic, and thermodynamic mechanisms in the MB-RCL adsorption process were examined.

2 Materials and Methods

2.1 Adsorbent Preparation and Characterization

RCL was collected from the campus of Kafkas University in Turkey. The dirt and impurities were removed using pure water, after which the plant stem was first sun dried and then dried in an oven at 105 °C for 24 h. The dried stems were then ground using a grinder and sieved, and the parts < 0.425 mm were stored in closed containers for the adsorption experiments. The characterization of the adsorbent was performed using BET (Micromeritics-3 Flex), FTIR (Bruker VERTEX 70v), SEM-EDX (Zeiss Sigma 300), and XRD (PANalytical Empyrean XRD) analyses. Point of zero charge (pHpzc) was determined, as reported by Benkadour et al. (2018).

2.2 Adsorbate and Adsorption Experiments

MB has a molecular weight of 320 g/mol, a chemical formula of $C_{16}H_{18}ClN_3S$, and a wavelength is 665 nm. The studied MB concentrations were prepared from a 1000-ppm stock solution. Experiments were carried out at 170 rpm in temperature-controlled shakers with 50 mL MB solution at known concentrations (40–160 mg/L) in 250-mL beakers. After adsorption, the samples were centrifuged at 5000 rpm for 10 min, and the MB concentration was determined using the MAPADA V1100D UV-visible

spectrophotometer. The initial pH values of the MB solutions were adjusted using 0.1 N NaOH and HCl solutions. The percentage and amount of adsorbed MB were determined using Eqs. (1), (2), and (3) below:

$$\%R = \frac{C_o - C_e}{C_o} \times 100 \quad (1)$$

$$q_e = \frac{\left(C_o - C_e\right) \times V}{m} \quad (2)$$

$$q_t = \frac{\left(C_o - C_t\right) \times V}{m} \quad (3)$$

where C_o, C_e, and C_t (mg/L) denote the initial concentration of MB, the MB concentration at equilibrium, and the MB concentration at any time (t), respectively; V indicates the solution volume (L); and m indicates the adsorbent amount (g).

3 Results and Discussion

3.1 Characterization of the Adsorbent

The specific surface area of the RCL analyzed using the BET method was found to be 0.1742 m^2/g, the mean pore diameter was 17.40 nm, and the total pore volume was 0.000758 cm^3/g. Because the average pore diameter was between 2 and 50 nm, the structure was mesoporous (Jawad et al. 2022).

The FTIR spectrum of RCL and MB-RCL are given in Fig. 1. The peak at 3319 cm^{-1} is attributed to the presence of O–H stretch. The peak at 2902 cm^{-1} represents the C–H stretches in cellulose and hemicellulose (Banerjee et al. 2016). The peak at 1728 cm^{-1} is attributed to the stretching vibration of C=O (Jin et al. 2019). The peak at 1589 cm^{-1} indicates C=C stresses in the aromatic rings. The band at 1220 cm^{-1} corresponds to the C–O stresses in the hemicellulose. The strong band at 1018 cm^{-1} corresponds to the vibrational stresses of C–O, C–C, and C–O–C in cellulose, hemicellulose, and lignin, respectively (Chan et al. 2016). Although the –OH and –C–H groups indicate the presence of cellulose and lignin, the -C=O groups indicate the presence of hemicellulose.

The XRD graph showing the crystallographic structure of RCL is given in Fig. 2. The apparent peaks between 2θ =15~40° indicate that RCL has a polycrystalline structure (Z. Li et al. 2018). The peaks at 2θ =15 and 22° are the characteristic peaks that represent the crystal structure of the lignocellulosic parts (Kupeta et al. 2018; Özdemir 2019).

SEM analysis was performed to evaluate the surface morphology of RCL before and after adsorption. Figure 3a shows the rough heterogeneous

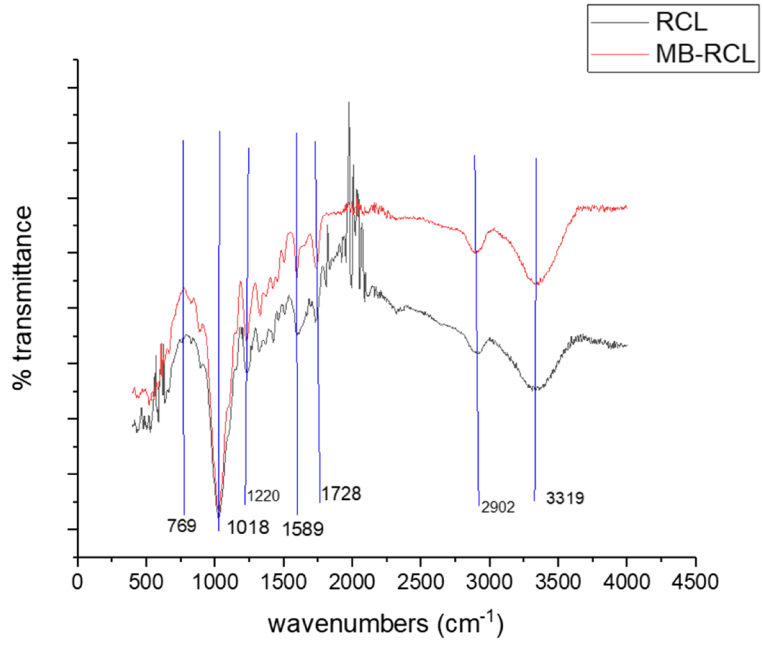

Fig. 1 Fourier transform infrared (FTIR) of *Rumex crispus* L. and MB-RCL

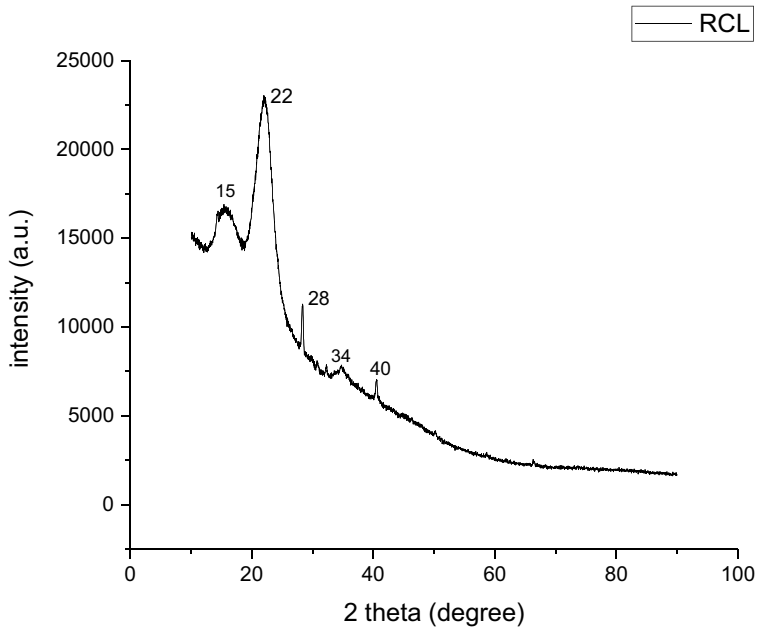

Fig. 2 X-ray diffraction (XRD) spectra of *Rumex crispus* L.

surface structure of RCL composed of scales and pores. This structure is important for adsorption success. Figure 3b shows that the adsorbent surface is filled with MB after adsorption, forming a smoother surface.

3.2 The Point of Zero Charge

The point of zero charge (pHpzc) for RCL adsorbent was calculated based on the reported method (Benkaddour et al. 2018). A 0.1 g RCL added to 95 ml NaCl solution and the pH suspension was adjusted to 2–10 by adding 0.1 N HCl and NaOH. The solution stirred for 24 h in the orbital shaker. Finally, the final pH values of the solutions were measured. The pHzpc of the sample was determined by plotting ΔpH (final pH–initial pH) versus pHi. As seen in Fig. 4, the pHzpc value of RCL was determined as 4.8.

3.3 Effects of Variation of Adsorbent Dosage

The effect of the amount of RCL used was investigated by changing the adsorbent/adsorbate ratio ranging from 0.5 to 6 g/L (Fig. 5). It was observed that the efficiency of MB removal surged from 68 to 90% with an increase in the adsorbent dose from 0.5 to 2.0 g/L; however, no change was observed at > 2.0 g/L. Thus, the highest adsorbent dose was determined to be 2.0 g/L in the present study; however, as the adsorption adsorbent/adsorbate ratio increased, the adsorption capacity decreased (Kızıltaş 2022). In adsorption experiments conducted at a constant volume, it was expected that the adsorption efficiency would increase with an increase in the amount of adsorbent because that increase would lead to an increase in the number and surface area of the active sites; however, after a specific point and because the adsorbent material agglomerates over its active sites, MB was prevented from reaching all these active sites and MB removal efficiency remained constant (Fernández-López et al. 2019).

3.4 Effect of Initial pH on Adsorption

Figure 6 shows the effect of the initial pH on adsorption. The effect of the initial pH on adsorption was studied by adding 2 g/L adsorbent to 50 mL MB solution (initial concentration = 80 mg/L). The adsorption experiments were conducted for 60 min while varying the pH from 3 to 10 to investigate the adsorption of MB by RCL. While 15.99 mg/g MB was adsorbed at pH = 3, there was a significant increase at pH = 4 adsorbent loading after reaching equilibrium [q_e] = 31.98 mg/g, and the highest value was reached at approximately pH = 7 (q_e = 34 mg/g); no change was observed at higher pH levels. pHpzc, the point at

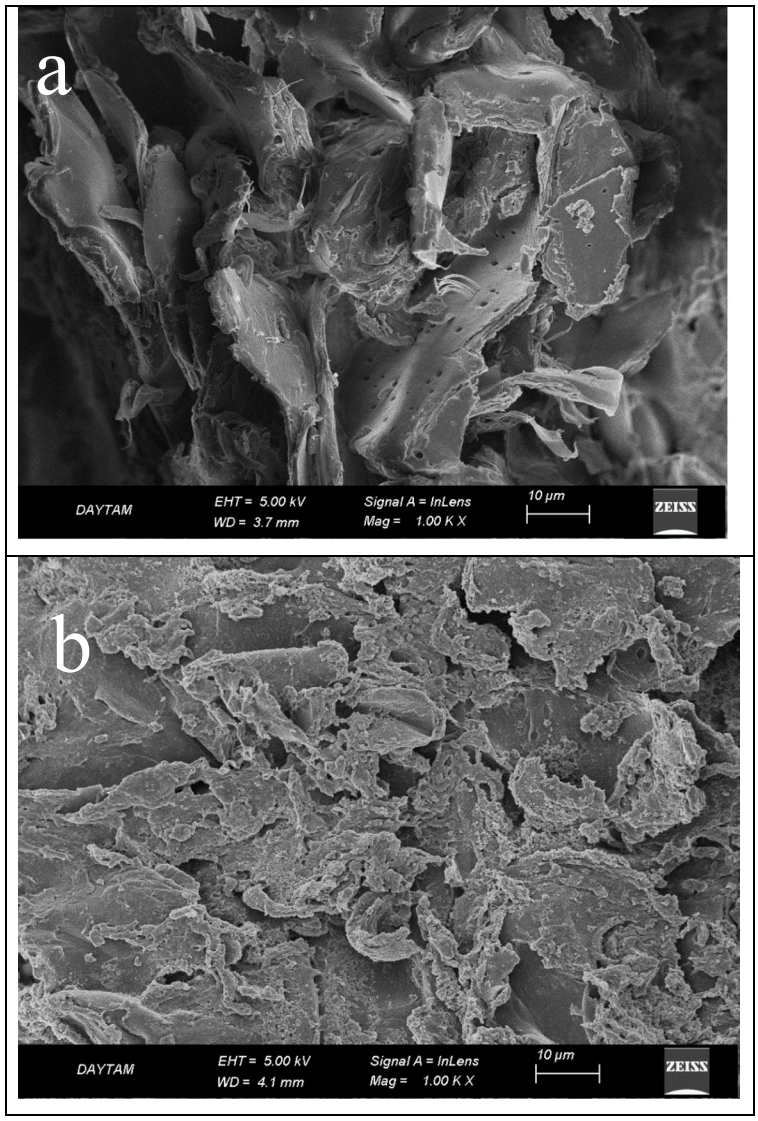

Fig. 3 Scanning electron microscopy images. **a** *Rumex crispus* L. and **b** methylene blue loaded *Rumex crispus* L. (MB-RCL)

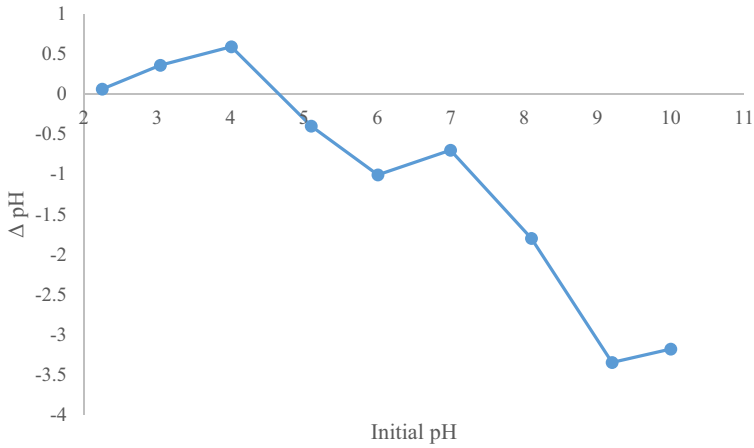

Fig. 4 The pH at point of zero charge (pHpzc) of *Rumex crispus* L. (2 g/L, 170 rpm, 20 °C, 24 h)

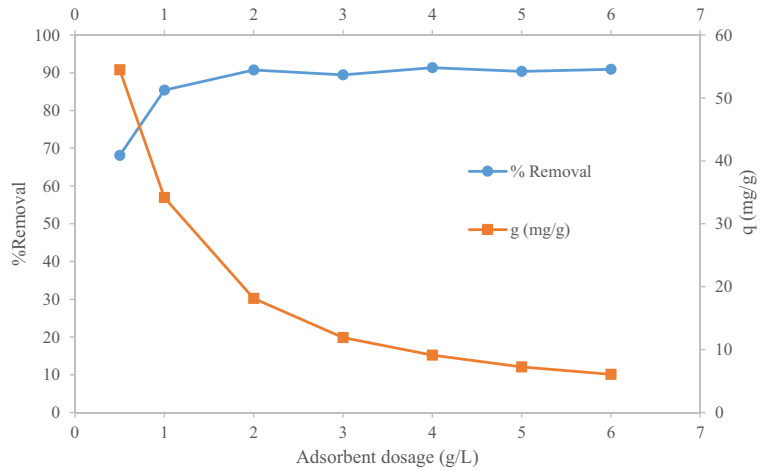

Fig. 5 Effect of adsorbent amount (C_0 = 40 mg/L, 170 rpm, free pH, 20 °C, 60 min)

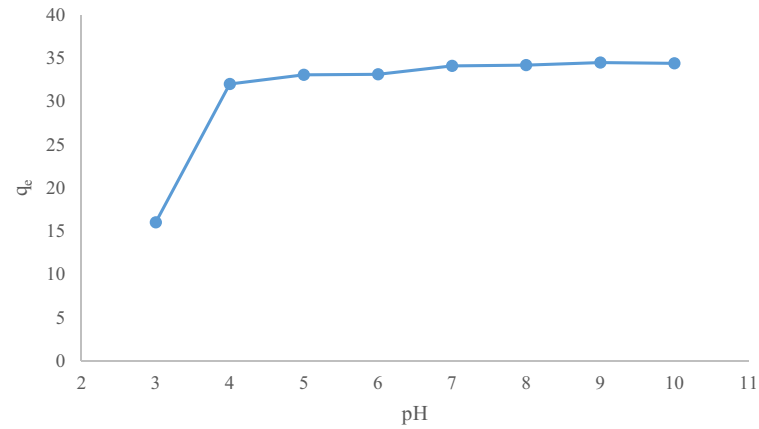

Fig. 6 Effect of pH (2 g/L, C_0 = 80 mg/L, 170 rpm, 20 °C, 60 min)

which the surface charge of the adsorbent is neutral, is an important parameter in adsorption. In Fig. 6, the pH values of RCL were changed to values between 3 and 10, and pHpzc was determined to be 4.8. When pH < pHpzc, the adsorbent surface was negatively charged, and when pH > pHpzc, it was positively charged. When pH < pHpzc, because the adsorbent surface was also positively charged, the repulsive forces between MB and the adsorbent surface limited the adsorption capacity (Akkari et al. 2021). When pH > 4.8, the surface of RCL was negatively charged; therefore, at higher pH values, cationic MB adhered more to the negatively charged adsorbent surface from electrostatic interaction. The free pH of MB was 6.4. Because this value was > pHzpc and there was no significant change in q_e at the initial pH > 6.4, the experiments were conducted at the free pH value.

3.5 Effect of MB Concentration on Adsorption

Figure 7 shows the effect of initial concentration. The experiments were conducted at initial concentrations of 40-80-120-160-200 mg/L. Experiments used RCL dosage 2 g/L, free pH, stirring speed of 170 rpm, and temperature of 20 °C. Eighty-nine percent of MB was adsorbed at an initial concentration of 40 mg/L, and the adsorption capacity was calculated as q_e = 17.79 mg/g. As the concentration increased, the percentage of adsorbed MB decreased to 56%. The amount of MB adsorbed was calculated as q_e = 56 mg/g. This was the result because there were more active sites at lower concentrations, and thus, the removal efficiency of the adsorbed MB increased; however, because there were a finite number of active sites, as the

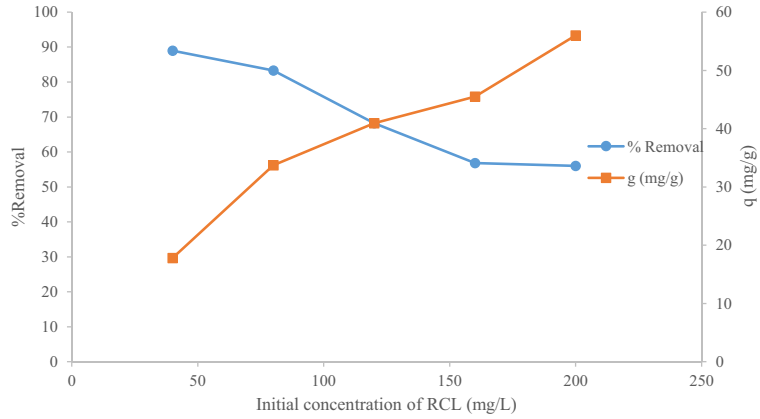

Fig. 7 Effect of concentration of *Rumex crispus* L. (2 g/L, 170 rpm, 20 °C, pH = 6.4, 60 min)

concentration increased, the active surfaces filled with MB and reached saturation, which reduced the removal efficiency (Kızıltaş and Aydın 2022). The initial concentration is the driving force in mass transfer; therefore, in the present study, as the concentration increased, the driving force between the solution phase and the solid phase increased and more MB was adsorbed per unit amount of adsorbent.

3.6 Effect of Contact Time on Adsorption

Figure 8 presents the effect of contact time from 0 to 60 min. The experiments were performed at 20 °C, free pH, and RCL dosage 2 g/L while initial concentration varying from 40 to160 mg/L. The adsorption was rapid within the first 20 min and increased slowly between 20 and 30 min. We observed that adsorption approached equilibrium within 30 min, with no change after that. This was the result of a fast adsorption rate from the large number of empty active sites at the beginning and a slower rate after saturation of these active sites over time (Sukla Baidya and Kumar 2021).

3.7 Effect of Temperature on Adsorption

The adsorption experiments were conducted from 293 to 313 °K to study the effect of temperature (Fig. 9). In experiments, RCL (adsorbent dosage 2 g/L) was added to 50 mL of an 80 mg/L MB solution for adsorption at free pH and 170 rpm. As the temperature increased, the amount of adsorbed MB decreased. This indicated that the adsorption process was exothermic, and the decrease in adsorption capacity with a temperature increase indicated that the desorption step became stronger with a temperature increase (Aral 2023). Moreover,

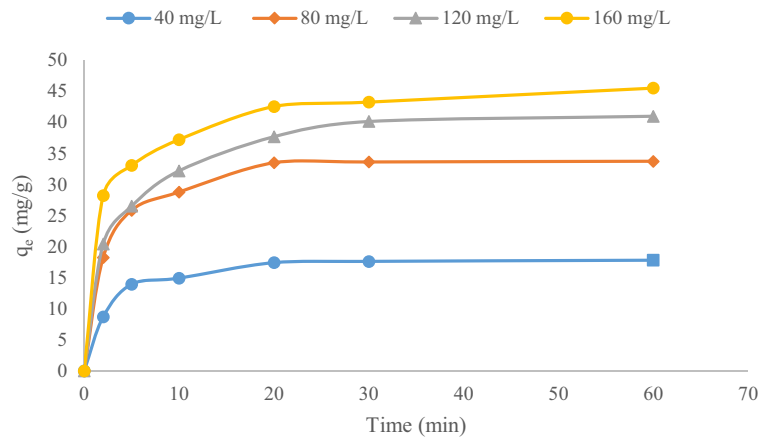

Fig. 8 Effect of contact time (2 g/L, 170 rpm, 20 °C, pH = 6.4)

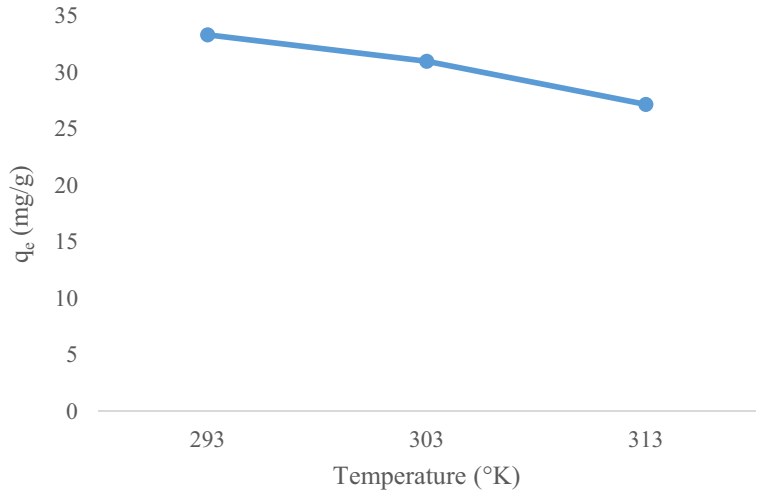

Fig. 9 Effect of temperature on adsorption

the adsorption forces between MB and the active sites on the RCL surface may have decreased with increasing temperature (Ofomaja and Ho 2007).

3.8 Adsorption Thermodynamics

To determine whether the adsorption process occurs spontaneously, the thermodynamic parameters of the adsorption of MB on RCL (ΔH [kJ/mol], ΔS [kJ/mol], ΔG [kJ/mol]) were calculated from the following equations. To find these values, a graph of 1/T against ln (K_d) was plotted (Fig. 10), and the slope and intercept give ΔH^0 and ΔS^0, respectively (Table 1).

$$K_d = \frac{q_e}{C_e} \tag{4}$$

$$\ln K_d = \frac{\Delta S^0}{R} - \frac{\Delta H^0}{RT} \tag{5}$$

$$\Delta G^0 = \Delta H^0 - T\Delta S^0 \tag{6}$$

where K_c is the distribution constant of the adsorbate and R is the universal gas constant (8.314 J/mol K).

The negative ΔH^0 indicated that the adsorption is exothermic, and the negative ΔS^0 value indicated that the randomness at the adsorbate–adsorbent interface decreased. The negative ΔG^0 indicated that the adsorption was spontaneous, while ΔG^0 increased as the temperature increased, indicating that there was a decrease in the spontaneity of the adsorption process with the increase in temperature. The fact that the ΔG^0 is between − 20 and 0 kJ/mol implies that the adsorption takes place physically (Auta and Hameed 2013; Lacin et al. 2019).

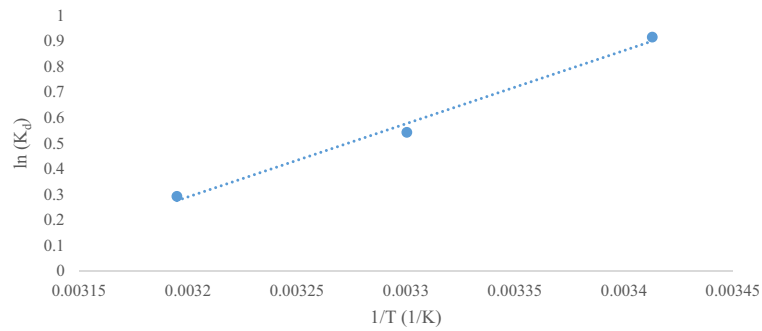

Fig. 10 ln(K_d) vs. 1/T

Table 1 Thermodynamic parameters of adsorption

T (°K)	ΔH^0 (kJ/mol)	ΔS^0 (kJ/mol)	ΔG^0 (kJ/mol)
293	− 23.8	− 0.074	− 2.19
303			− 1.45
313			− 0.72

3.9 Kinetic Models

The dynamic relationship between MB and RCL was tested using kinetic models by examining the correlation between adsorption rate and time, which enabled us to determine the time required for the reaction to reach adsorption equilibrium. For this purpose, four different kinetic models were tested, the correlation coefficients were compared, and the best-fit model was determined. Pseudo-first-order, pseudo-second-order, intraparticle diffusion, and Elovich kinetic models were used to determine the control mechanisms in adsorption processes. The equations for these models are given below.

Pseudo-first-order kinetic model (Lagergren 1898)**:**

$$\log\left(q_e - q_t\right) = \log q_e - \frac{k_1\, t}{2.303} \tag{7}$$

Equilibrium rate constant (k_1) was calculated from the slope of $\log(q_e - q_t)$ vs t graph.

q_e ver. q_t, denotes the adsorption capacity (mg/g) at equilibrium and time t, k_1 denotes the equilibrium rate constant (min^{-1}), and t denotes contact time.

Pseudo-second-order model (Ho and McKay 1999)**:**

$$\frac{t}{q_t} = \frac{1}{k_2 q_e^2} + \frac{1}{q_e\, t} \tag{8}$$

where q_e was calculated from the slope of $\frac{t}{q_t}$ vs. t graph, and from the intercept, the equilibrium rate constant of the pseudo-second-order (k_2) was calculated.

Intraparticle diffusion model (Weber and Morris 1963)**:**

$$q_t = k_{id} t^{0.5} + C \tag{9}$$

The intercept of the q_t vs. $t^{0.5}$ graph gives C, and its slope gives the intraparticle diffusion rate (k_{id}) (mg/g $min^{0.5}$).

C is a constant related to the thickness of the boundary layer. A large C value indicates that the contribution of surface adsorption is high in the step that controls the rate. If the graph of Eq. (9) passes through the origin, it means that the step controlling the rate is the intraparticle diffusion model; if it does not pass through the origin, it is not just the intraparticle diffusion model (Auta and Hameed 2013).

Elovich model (Mashkoor and Nasar 2019)**:**

$$q_t = \frac{1}{\beta}\ln(\alpha\beta) + \frac{1}{\beta}\ln(t) \tag{10}$$

where $\left(\frac{1}{\beta}\right)$ and $\frac{1}{\beta}\ln(\alpha\beta)$ were calculated from the slope and intercept between q_t vs. ln(t). Here, α was the initial adsorption rate (mg/g $min^{0.5}$); β was the desorption constant (g/mg).

The kinetic studies on the adsorption of MB on RCL are shown in Fig. 11. The constants and correlation coefficients calculated from the graphs of these kinetic models are listed in Table 2. The adsorption mechanism can be explained using the pseudo-second-order kinetic model because the correlation coefficient approaches one ($R^2 > 0.99$). Given that the controlling mechanism of the adsorption process is pseudo-second-order, the adsorption was chemical (i.e., there is ion sharing or ion transfer between MB and RCL) (Fan et al. 2017). Table 2 indicates that the rate constant decreased with an increase in concentration, which is explained as follows: Mass transfer does not occur effectively at low concentrations; therefore, reaching equilibrium takes time at high concentrations. In addition, the increase in C with increasing concentration in the intraparticle diffusion model indicated that the thickness of the boundary layer increased. Furthermore, given that the step that did not pass through the origin, the step controlling the rate was not only the intraparticle diffusion model, which implies that external diffusion, or surface adsorption, and liquid film diffusion also had an effect. Thus, it can be said that the adsorption mechanism was controlled by both intraparticle and liquid film diffusion. We observed that the correlation coefficients for the Elovich kinetic model were high. This model presumes that the adsorbent surface has heterogeneous energy in chemisorption processes (Wang et al. 2019), which confirmed that

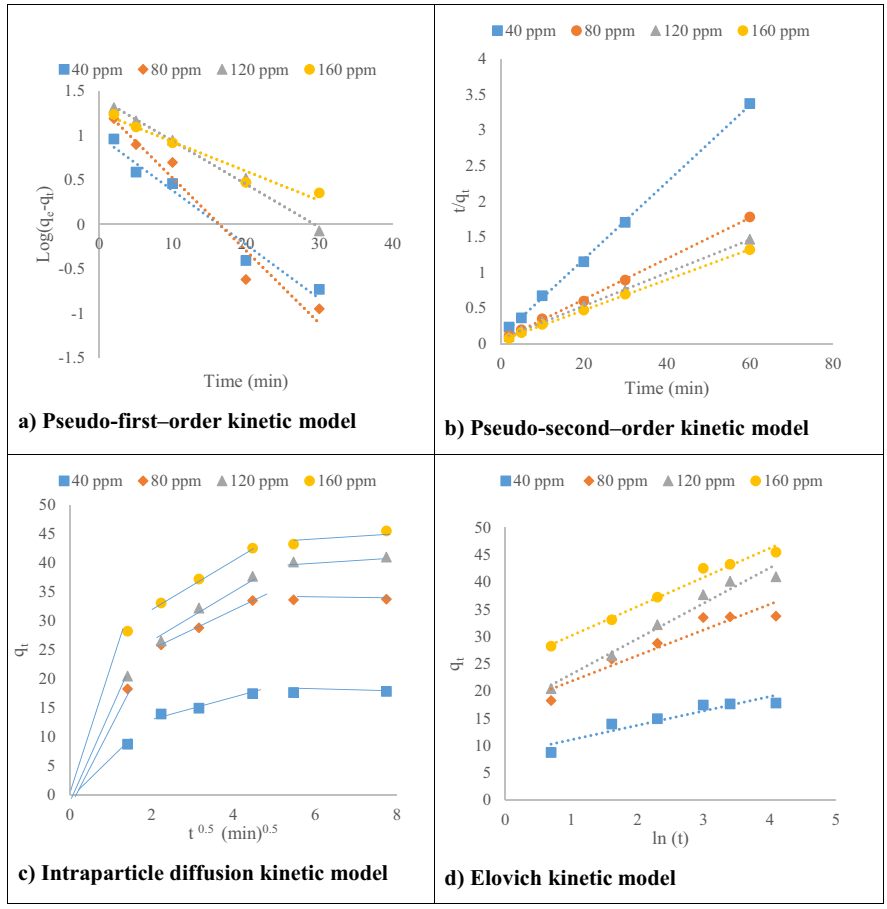

Fig. 11 Kinetic models

Table 2 Parameters of kinetic models

	Pseudo-first-order constants			**Pseudo-second-order constants**		
C_0 (mg/L) (mg/L)	q_e (mg/g)	k_1 (min^{-1})	R^2	q_e (mg/g)	k_2(g/mg min)	R^2
40	9.71	0.13979	0.966	18.45	0.02949	0.999
80	21.62	0.18769	0.955	34.84	0.01790	0.999
120	26.36	0.11146	0.995	42.92	0.00844	0.999
160	17.99	0.07576	0.957	46.73	0.01050	0.999
	Intraparticle diffusion constants			**Elovich constants**		
C_0 (mg/L)	k_{id} (mg/g $min^{0.5}$)	C	R^2	α	β	R^2
40	1.25	9.93	0.689	63.158	0.378	0.878
80	2.24	19.78	0.712	177.912	0.212	0.899
120	3.24	19.72	0.839	83.116	0.153	0.968
160	2.69	27.27	0.870	556.704	0.187	0.979

the mechanism on the surface with heterogeneous energy does not correlate with the pseudo-first-order model but is in agreement with the pseudo-second-order kinetic model. In addition, Table 2 shows that the initial adsorption rate (α) was considerably larger than the desorption rate (β). Low desorption rates indicated interactions between MB and the C sites on RCL (Brito et al. 2018).

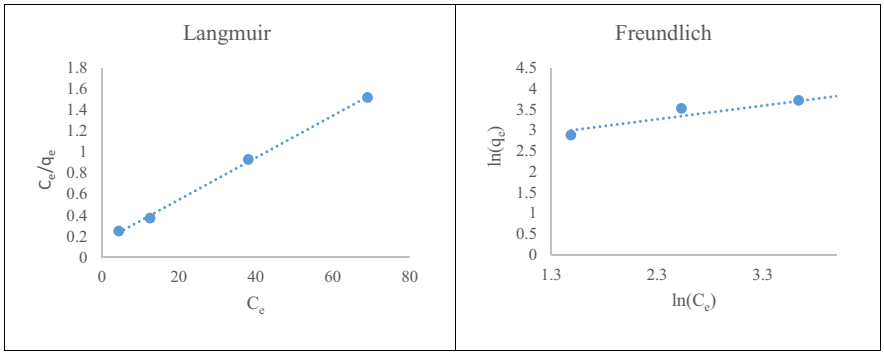

Fig. 12 Adsorption isotherms

Table 3 Values of parameters of Isotherm models

Langmuir	q_{max} (mg/g)	K_L	R^2
	50	0.135	0.998
Freundlich	K_F	n	R^2
	12.25	3.045	0.901

3.10 Isotherm Studies

Adsorption isotherms are the indicators by which adsorption capacity and adsorbent–adsorbate behavior can be determined. Langmuir and Freundlich models were tested on the adsorption process between MB and RCL. The linear equation for the Langmuir isotherm, which presumes that the adsorption processes are monolayer, and the sites are homogeneous and have equal energies, is given below (Langmuir 1918):

$$\frac{C_e}{q_e} = \frac{1}{q_{max}K_L} + \frac{C_e}{q_{max}} \tag{11}$$

where K_L is obtained from the slope of $\frac{C_e}{q_e}$ vs. C_e graph and q_{max} is obtained from the intercept. The q_e is the amount of adsorbate per unit adsorbent mass (mg/g) at equilibrium, q_{max} is the maximum adsorption capacity of the adsorbent (mg/g), C_e is the dye concentration in solution at equilibrium (mg/L), and K_L is the Langmuir adsorption constant (L/mg).

The characteristic R_L value of the Langmuir isotherm is calculated from (Eq. 12):

Table 4 q_{max}, kinetic, and isotherm data on MB for some adsorbents

Adsorbent	Q_{max} (mg/g)	Isotherm/kinetic model	Reference
Arginine-modified activated carbon	219.9	L-PSO	(Naushad et al. 2019)
Walnut shell powder	178.9	L-PSO	(Miyah et al. 2018)
Chemically modified lychee seed	124.5	L-PSO	(Sahu et al. 2020)
litchi leaves powder	119,76	L-PSO	(Yadav et al. 2023)
Acid-washed black cumin seed powder	73.529	L-PSO	(Siddiqui et al. 2018)
Crisp persimmon peel	59.72	L-PSO	(Xie et al. 2022)
Algerian palygorskite	57.47	L-PSO	(Dali Youcef et al. 2019)
Coconut shell	50.6	F-PSO	(Jawad et al. 2020)
RCL	50	L-PSO	This study
Chemically modified pine nut shells	39.73	L-PSO	(Naushad et al. 2016)
Lignin-chitosan blend	36.25	L-PSO	(Rezakazemi and Shirazian 2019)
Carboxymethyl cellulose/k-carrageenan/ montmorillonite beads	12.25	L-PSO	(Liu et al. 2018)

Notes: *MB* methylene blue, *F* Freundlich, *L* Langmuir, *PSO* pseudo-second order

$$R_L = \frac{1}{1 + K_L C_0} \tag{12}$$

where C_0 was the highest initial concentration of the dye (mg/L). $R_L > 1$ that adsorption is unfavorable, $R_L = 1$ that it is linear, $0 < R_L < 1$ that it is favorable, and $R_L = 0$ that it is reversible.

The linear equation for the Freundlich isotherm (Freundlich 1906) is given in (Eq. 13):

$$\ln q_e = \ln K_F + \left(\frac{1}{n}\right) \ln C_e \tag{13}$$

The slope of $\ln(q_e)$ vs $\ln(C_e)$ gives 1/n, and K_F is calculated from its intercept.

Figure 12 shows the graphs of these isotherms. The constants calculated from these graphs are presented in Table 3.

A comparison of correlation coefficients indicated that the Langmuir isotherm described the adsorption process very well ($R^2 > 0.99$). We suggest that the adsorption of MB on RCL was a monolayer adsorption and that the bound sites were homogeneous and had the same amount of energy. The maximum adsorption capacity was 50 mg/g. The separation factor R_L was varied from 0.156 to 0.044 for 40 to 160 mg/L, respectively. $R_L < 1$ indicated that the adsorption process of MB on RCL was favorable. In addition, the decrease in R_L with an increase in the initial concentration of RCL indicated that the adsorption process was positively affected.

The Freundlich isotherm is an empirical equation that presumes that the adsorbent surface has heterogeneous energies. A value of $n > 1$ indicates that adsorption is favorable. The K_F adsorption capacity in the present study was 12.25 mg/g, and the heterogeneity factor n value was c 3.045. A high n value implies that the surface is homogeneous and the adsorption process is favorable (Eslami et al. 2018). The q_{max} for MB for some different adsorbents and the data from the isotherm and kinetic models with which it is compatible are presented in Table 4.

4 Conclusion

In this study, the adsorbent obtained from the stems of RCL, a plant that grows naturally but often decays and disappears because of its quite limited use, was used to remove MB from an aqueous solution. The characteristic structure of RCL was investigated using BET, FTIR, XRD, and SEM analyses. As the amount of adsorbent increased (0.5–2 g/L), the removal% did not change after 0.2 g/L, but the adsorption capacity decreased. In pH experiments, while the adsorption capacity increased from pH 3 to 7, the adsorption capacity did not change after pH 7. The MB-RCL adsorption process reached equilibrium in 30 min. It was observed that the amount of MB adsorbed increased as the concentration and temperature increased. The kinetic data showed that the pseudo-second-order model was the best fit ($R^2 = 0.999$). The Langmuir isotherm model was found the best described the adsorption process. According to this model, the maximum adsorption capacity of the RCL monolayer was 50 mg/g at 293 K and free pH. A negative ΔG^0 indicated that the adsorption process was voluntary, a negative ΔH^0 indicated that the adsorption was exothermic, and a negative ΔS^0 indicated that the randomness decreased at the adsorbate-adsorbent interface ($\Delta G^0 = -2.19$ to -0.72 kJ/mol, $\Delta H^0 = -23.8$ kJ/mol, $\Delta S^0 = -0.074$ kJ/mol). When RCL was used as an adsorbent, it removed 90% of the MB at 40 ppm in solution; therefore, as an economical and abundant biomass, RCL can be used as a potential bio-adsorbent to remove MB from aqueous solution.

Data Availability All data generated or analyzed during this study are included in this published article.

Declarations

Competing Interests The author declares no competing interests.

References

Abdulrazzaq, N. N., Al-Sabbagh, B. H., & Shanshool, H. A. (2021). Coupling of electrocoagulation and microflotation for the removal of textile dyes from aqueous solutions. *Journal of Water Process Engineering, 40*, 101906. https://doi.org/10.1016/j.jwpe.2020.101906

Akkari, I., Graba, Z., Bezzi, N., Merzeg, F. A., Bait, N., & Ferhati, A. (2021). Raw pomegranate peel as promise efficient biosorbent for the removal of Basic Red 46 dye: Equilibrium, kinetic, and thermodynamic studies. *Biomass Conversion and Biorefinery, 13*(9), 8047–8060. https://doi.org/10.1007/s13399-021-01620-9

Aral, S. (2023). Production of effective activated carbon from scotch pine bark and investigation of the adsorption properties. *Iranian journal of chemistry and chemical engineering*. https://doi.org/10.30492/ijcce.2023.1995732.5912

Auta, M., & Hameed, B. H. (2013). Acid modified local clay beads as effective low-cost adsorbent for dynamic adsorption of methylene blue. *Journal of Industrial and Engineering Chemistry, 19*(4), 1153–1161. https://doi.org/10.1016/j.jiec.2012.12.012

Badvi, K., & Javanbakht, V. (2021). Enhanced photocatalytic degradation of dye contaminants with TiO2 immobilized on ZSM-5 zeolite modified with nickel nanoparticles. *Journal of Cleaner Production, 280*, 124518. https://doi.org/10.1016/j.jclepro.2020.124518

Banerjee, S., Sharma, G. C., Gautam, R. K., Chattopadhyaya, M. C., Upadhyay, S. N., & Sharma, Y. C. (2016). Removal of Malachite Green, a hazardous dye from aqueous solutions using Avena sativa (oat) hull as a potential adsorbent. *Journal of Molecular Liquids, 213*, 162–172.

Beluci, N. D., Mateus, G. A., Miyashiro, C. S., Homem, N. C., Gomes, R. G., Fagundes-Klen, M. R., Bergamasco, R., & Vieira, A. M. (2019). Hybrid treatment of coagulation/flocculation process followed by ultrafiltration in TIO2-modified membranes to improve the removal of reactive black 5 dye. *Science of the Total Environment, 664*, 222–229. https://doi.org/10.1016/j.scitotenv.2019.01.199

Benkaddour, S., Slimani, R., Hiyane, H., El Ouahabi, I., Hachoumi, I., El Antri, S., & Lazar, S. (2018). Removal of reactive yellow 145 by adsorption onto treated watermelon seeds: Kinetic and isotherm studies. *Sustainable Chemistry and Pharmacy, 10*, 16–21. https://doi.org/10.1016/j.scp.2018.08.003

Bhandari, G. S., & Park, C.-W. (2022). Molecular evidence for natural hybridization between Rumex crispus and R. obtusifolius (Polygonaceae) in Korea. *Scientific Reports, 12*(1), 5423. https://doi.org/10.1038/s41598-022-09292-9

Bingöl, M. S. (2022). Effects of prepared gadolinium oxide-doped chitosan/PVA hydrogels on Congo red removal in water. *Water, Air, & Soil Pollution, 233*(10), 410. https://doi.org/10.1007/s11270-022-05884-3

Brito, M. J. P., Veloso, C. M., Santos, L. S., Bonomo, R. C. F., & Fontan, R. D. C. I. (2018). Adsorption of the textile dye Dianix® royal blue CC onto carbons obtained from yellow mombin fruit stones and activated with KOH and H3PO4: Kinetics, adsorption equilibrium and thermodynamic studies. *Powder Technology, 339*, 334–343. https://doi.org/10.1016/j.powtec.2018.08.017

Chan, S.-L., Tan, Y. P., Abdullah, A. H., & Ong, S.-T. (2016). Equilibrium, kinetic and thermodynamic studies of a new potential biosorbent for the removal of Basic Blue 3 and Congo Red dyes: Pineapple (Ananas comosus) plant stem. *Journal of the Taiwan Institute of Chemical Engineers, 61*, 306–315. https://doi.org/10.1016/j.jtice.2016.01.010

Cheruiyot, G. K., Wanyonyi, W. C., Kiplimo, J. J., & Maina, E. N. (2019). Adsorption of toxic crystal violet dye using coffee husks: Equilibrium, kinetics and thermodynamics study. *Scientific African, 5*, e00116. https://doi.org/10.1016/j.sciaf.2019.e00116

Eldeeb, T. M., Aigbe, U. O., Ukhurebor, K. E., Onyancha, R. B., El-Nemr, M. A., Hassaan, M. A., et al. (2022). Adsorption of methylene blue (MB) dye on ozone, purified and sonicated sawdust biochars. *Biomass Conversion and Biorefinery*. https://doi.org/10.1007/s13399-022-03015-w

Eslami, P. A., Kamboh, M. A., Nodeh, H. R., & Ibrahim, W. A. W. (2018). Equilibrium and kinetic study of novel methyltrimethoxysilane magnetic titanium dioxide nanocomposite for methylene blue adsorption from aqueous media. *Applied Organometallic Chemistry, 32*(6), e4331. https://doi.org/10.1002/aoc.4331

Fabryanty, R., Valencia, C., Soetaredjo, F. E., Putro, J. N., Santoso, S. P., Kurniawan, A., et al. (2017). Removal of crystal violet dye by adsorption using bentonite – alginate composite. *Journal of Environmental Chemical Engineering, 5*(6), 5677–5687. https://doi.org/10.1016/j.jece.2017.10.057

Fan, S., Wang, Y., Wang, Z., Tang, J., Tang, J., & Li, X. (2017). Removal of methylene blue from aqueous solution by sewage sludge-derived biochar: Adsorption kinetics, equilibrium, thermodynamics and mechanism. *Journal of Environmental Chemical Engineering, 5*(1), 601–611. https://doi.org/10.1016/j.jece.2016.12.019

Feduraev, P., Chupakhina, G., Maslennikov, P., Tacenko, N., & Skrypnik, L. (2019). Variation in phenolic compounds content and antioxidant activity of different plant organs from Rumex crispus L. and Rumex obtusifolius L. at different growth stages. *Antioxidants, 8*(7), 237. https://doi.org/10.3390/antiox8070237

Fernández-López, J. A., Angosto, J. M., Roca, M. J., & Doval Miñarro, M. (2019). Taguchi design-based enhancement of heavy metals bioremoval by agroindustrial waste biomass from artichoke. *Science of the Total Environment, 653*, 55–63. https://doi.org/10.1016/j.scitotenv.2018.10.343

Freundlich, H. M. F. (1906). Over the adsorption in solution. *The Journal of Physical Chemistry, 57*, 385–471.

Ho, Y. S., & McKay, G. (1999). Pseudo-second order model for sorption processes. *Process Biochemistry, 34*(5), 451–465. https://doi.org/10.1016/S0032-9592(98)00112-5

Idris, O. A., Wintola, O. A., & Afolayan, A. J. (2017). Phytochemical and antioxidant activities of Rumex crispus L. in treatment of gastrointestinal helminths in Eastern Cape Province, South Africa. *Asian Pacific Journal of Tropical Biomedicine, 7*(12), 1071–1078. https://doi.org/10.1016/j.apjtb.2017.10.008

Isik, B., Ugraskan, V., Cakar, F., & Yazici, O. (2022). A comparative study on the adsorption of toxic cationic dyes by Judas tree (Cercis siliquastrum) seeds. *Biomass Conversion and Biorefinery*. https://doi.org/10.1007/s13399-022-02679-8

Jawad, A. H., Razuan, R., Appaturi, J. N., & Wilson, L. D. (2019). Adsorption and mechanism study for methylene blue dye removal with carbonized watermelon (Citrullus lanatus) rind prepared via one-step liquid phase H2SO4 activation. *Surfaces and Interfaces, 16*, 76–84. https://doi.org/10.1016/j.surfin.2019.04.012

Jawad, A. H., Saber, S. E. M., Abdulhameed, A. S., Reghioua, A., ALOthman, Z. A., & Wilson, L. D. (2022). Mesoporous activated carbon from mangosteen (Garcinia mangostana) peels by H3PO4 assisted microwave: Optimization, characterization, and adsorption mechanism for

methylene blue dye removal. *Diamond and Related Materials, 129*, 109389. https://doi.org/10.1016/j.diamond.2022.109389

Jin, Y., Zeng, C., Lü, Q.-F., & Yu, Y. (2019). Efficient adsorption of methylene blue and lead ions in aqueous solutions by 5-sulfosalicylic acid modified lignin. *International Journal of Biological Macromolecules, 123*, 50–58. https://doi.org/10.1016/j.ijbiomac.2018.10.213

Khan, S. A., & Khan, T. A. (2021). Clay-hydrogel nanocomposites for adsorptive amputation of environmental contaminants from aqueous phase: A review. *Journal of Environmental Chemical Engineering, 9*(4), 105575. https://doi.org/10.1016/j.jece.2021.105575

Kızıltaş, H. (2022). Production of highly effective adsorbent from tea waste, and its adsorption behaviors and characteristics for the removal of Rhodamine B. International Journal of Environmental Analytical Chemistry, 0(0), 1–20. doi:https://doi.org/10.1080/03067319.2022.2047181

Kızıltaş, H., & Aydın, Ö. (2022). Removal of Orange G dye using peanut shells activated carbon: A green synthesis approach. International Journal of Environmental Analytical Chemistry, 0(0), 1–21. doi:https://doi.org/10.1080/03067319.2022.2098476

Kupeta, A. J. K., Naidoo, E. B., & Ofomaja, A. E. (2018). Kinetics and equilibrium study of 2-nitrophenol adsorption onto polyurethane cross-linked pine cone biomass. *Journal of Cleaner Production, 179*, 191–209. https://doi.org/10.1016/j.jclepro.2018.01.034

Lacin, O., Haghighatnia, A., Demir, F., & Sevim, F. (2019). Adsorption characteristics and behaviors of natural red clay for removal of BY28 from aqueous solutions. *IJTSRD, 3*(2), 1037–1047. https://doi.org/10.31142/ijtsrd21544

Lagergren, S. K. (1898). About the theory of so-called adsorption of soluble substances. *Sven. Vetenskapsakad. Handingarl, 24*, 1–39.

Langmuir, I. (1918). The adsorption of gases on plane surfaces of glass, mica and platinum. *Journal of the American Chemical Society, 40*(9), 1361–1403.

Li, J., Yuan, S., Zhu, J., & Van der Bruggen, B. (2019). High-flux, antibacterial composite membranes via polydopamine-assisted PEI-TiO2/Ag modification for dye removal. *Chemical Engineering Journal, 373*, 275–284. https://doi.org/10.1016/j.cej.2019.05.048

Li, Z., Wang, G., Zhai, K., He, C., Li, Q., & Guo, P. (2018). Methylene blue adsorption from aqueous solution by loofah sponge-based porous carbons. *Colloids and Surfaces A: Physicochemical and Engineering Aspects, 538*, 28–35. https://doi.org/10.1016/j.colsurfa.2017.10.046

Mashkoor, F., & Nasar, A. (2019). Preparation, characterization and adsorption studies of the chemically modified Luffa aegyptica peel as a potential adsorbent for the removal of malachite green from aqueous solution. *Journal of Molecular Liquids, 274*, 315–327. https://doi.org/10.1016/j.molliq.2018.10.119

Motejadded Emrooz, H. B., Maleki, M., Rashidi, A., & Shokouhimehr, M. (2021). Adsorption mechanism of a cationic dye on a biomass-derived micro- and mesoporous carbon: Structural, kinetic, and equilibrium insight. *Biomass Conversion and Biorefinery, 11*(3), 943–954. https://doi.org/10.1007/s13399-019-00584-1

Muniyasamy, A., Sivaporul, G., Gopinath, A., Lakshmanan, R., Altaee, A., Achary, A., & Velayudhaperumal Chellam, P. (2020). Process development for the degradation of textile azo dyes (mono-, di-, poly-) by advanced oxidation process - Ozonation: Experimental & partial derivative modelling approach. *Journal of Environmental Management, 265*, 110397. https://doi.org/10.1016/j.jenvman.2020.110397

Mussa, Z. H., Al-Ameer, L. R., Al-Qaim, F. F., Deyab, I. F., Kamyab, H., & Chelliapan, S. (2023). A comprehensive review on adsorption of methylene blue dye using leaf waste as a bio-sorbent: isotherm adsorption, kinetics, and thermodynamics studies. *Environmental Monitoring and Assessment, 195*(8), 940. https://doi.org/10.1007/s10661-023-11432-1

Nayak, A. K., & Pal, A. (2020). Utilization of lignocellulosic waste for acridine orange uptake: insights into multiparameter isotherms modeling with ANN-aimed formulation. *Journal of Environmental Engineering, 146*(9), 04020096. https://doi.org/10.1061/(ASCE)EE.1943-7870.0001762

Ofomaja, A. E., & Ho, Y.-S. (2007). Equilibrium sorption of anionic dye from aqueous solution by palm kernel fibre as sorbent. *Dyes and Pigments, 74*(1), 60–66. https://doi.org/10.1016/j.dyepig.2006.01.014

Özdemir, Ç. S. (2019). Equilibrium, kinetic, diffusion and thermodynamic applications for dye adsorption with pine cone. Separation Science and Technology, 0(0), 1–9. doi:https://doi.org/10.1080/01496395.2019.1565769

Sah, M. K., Edbey, K., EL-Hashani, A., Almshety, S., Mauro, L., Alomar, T. S., AlMasoud, N., & Bhattarai, A. (2022). Exploring the biosorption of methylene blue dye onto agricultural products: A critical review. *Separations, 9*(9), 256. https://doi.org/10.3390/separations9090256

Sarkar, S., Tiwari, N., Basu, A., Behera, M., Das, B., Chakrabortty, S., et al. (2021). Sorptive removal of malachite green from aqueous solution by magnetite/coir pith supported sodium alginate beads: Kinetics, isotherms, thermodynamics and parametric optimization. *Environmental Technology and Innovation, 24*, 101818. https://doi.org/10.1016/j.eti.2021.101818

Sukla Baidya, K., & Kumar, U. (2021). Adsorption of brilliant green dye from aqueous solution onto chemically modified areca nut husk. *South African Journal of Chemical Engineering, 35*, 33–43. https://doi.org/10.1016/j.sajce.2020.11.001

Sultana, H., Usman, M., ul Haq, A., & Mansha, A. (2021). Micellar enhanced flocculation for the effective removal of reactive yellow 160 from synthetic textile effluent. *Environmental Technology and Innovation, 24*, 101896. https://doi.org/10.1016/j.eti.2021.101896

Tang, X., Ran, G., Li, J., Zhang, Z., & Xiang, C. (2021). Extremely efficient and rapidly adsorb methylene blue using porous adsorbent prepared from waste paper: Kinetics and equilibrium studies. *Journal of Hazardous Materials, 402*, 123579. https://doi.org/10.1016/j.jhazmat.2020.123579

Thakur, S., Pandey, S., & Arotiba, O. A. (2016). Development of a sodium alginate-based organic/inorganic superabsorbent composite hydrogel for adsorption of methylene blue. *Carbohydrate Polymers, 153*, 34–46. https://doi.org/10.1016/j.carbpol.2016.06.104

Uzun, M., & Demirezer, L. O. (2019). Anti-aging power of Rumex crispus L.: Matrixmetalloproteinases inhibitor, sun protective and antioxidant. *South African Journal of Botany, 124*, 364–371. https://doi.org/10.1016/j.sajb.2019.05.028

Wang, B., Gao, B., & Wan, Y. (2019). Comparative study of calcium alginate, ball-milled biochar, and their composites on aqueous methylene blue adsorption. *Environmental Science and Pollution Research, 26*(12), 11535–11541. https://doi.org/10.1007/s11356-018-1497-1

Weber, W. J., & Morris, J. C. (1963). Kinetics of adsorption on carbon from solution. *Journal of the Sanitary Engineering Division, 89*(2), 31–59. https://doi.org/10.1061/JSEDAI.0000430

Xue, H., Wang, X., Xu, Q., Dhaouadi, F., Sellaoui, L., Seliem, M. K., et al. (2022). Adsorption of methylene blue from aqueous solution on activated carbons and composite prepared from an agricultural waste biomass: A comparative study by experimental and advanced modeling analysis. *Chemical Engineering Journal, 430*, 132801. https://doi.org/10.1016/j.cej.2021.132801

Zahirnejad, M., Ziarati, P., & Asgarpanah, J. (2017). The Efficiency of bio-adsorption of heavy metals from pharmaceutical effluent by Rumex crispus L. *Seed, 5*(3).